

---

Konrad-Zuse-Zentrum  
für Informationstechnik Berlin

Takustraße 7  
D-14195 Berlin-Dahlem  
Germany

ANDREA KRATZ, BJÖRN MEYER, INGRID HOTZ

# **A Visual Approach to Analysis of Stress Tensor Fields**

Submitted August 31, 2010

---

ZIB-Report 10-26 (August 2010)

# A Visual Approach to Analysis of Stress Tensor Fields

Andrea Kratz, Björn Meyer, and Ingrid Hotz

**Abstract**—We present a visual approach for the exploration of stress tensor fields. Therefore, we introduce the idea of multiple linked views to tensor visualization. In contrast to common tensor visualization methods that only provide a single view to the tensor field, we pursue the idea of providing various perspectives onto the data in attribute and object space. Especially in the context of stress tensors, advanced tensor visualization methods have a young tradition. Thus, we propose a combination of visualization techniques domain experts are used to with statistical views of tensor attributes. The application of this concept to tensor fields was achieved by extending the notion of shape space. It provides an intuitive way of finding tensor invariants that represent relevant physical properties. Using brushing techniques, the user can select features in attribute space, which are mapped to displayable entities in a three-dimensional hybrid visualization in object space. Volume rendering serves as context, while glyphs encode the whole tensor information in focus regions. Tensorlines can be included to emphasize directionally coherent features in the tensor field. We show that the benefit of such a multi-perspective approach is manifold. Foremost, it provides easy access to the complexity of tensor data. Moreover, including well-known analysis tools, such as Mohr diagrams, users can familiarize themselves gradually with novel visualization methods. Finally, by employing a focus-driven hybrid rendering, we significantly reduce clutter, which was a major problem of other three-dimensional tensor visualization methods.

**Index Terms**—



## 1 INTRODUCTION

The focus of this work is the analysis and visualization of 3D stress tensor fields, which express the response of a material to applied forces. Important application areas and their interest in such data are: In material science, a material's behavior under pressure is observed to examine its stability. Similar questions also arise in astrophysics. Rock fractures caused by tension or compression, for example, are analyzed in geosciences. A medical example is the simulation of an implant design's impact on the distribution of physiological stress inside a bone [1]. Common to most of these areas is the goal of finding regions where the inspected material tends to crack. Various failure models exist, but in general they are based on the analysis of large shear stresses. Besides understanding a physical phenomenon, tensor analysis can help to detect failures in simulations where tensors appear as intermediate product. In all these application areas, regions of interest are not necessarily known in advance. For this reason, powerful visual exploration and analysis tools are of high importance.

The complexity of tensor data makes them hard to visualize and interpret. Therefore, users tend to analyze tensor data via two-dimensional plots of derived scalars (data reduction). Although these plots simplify the analysis at first glance, they do not communicate the evolution of tensors over the whole field [2]. They might even fail to convey all information given by a single tensor. From a visualization point of view, the difficulty lies in depicting each tensor's complex information, especially for three-dimensional tensor fields.

Often, visualizations are restricted to two-dimensional slices (data projection), as three-dimensional visualizations tend to result in cluttered images. However, data reduction and data projection both reduce the complex information of the tensor field to a small subset. Thus, the richness of the data is not communicated.

A further challenge, for example in contrast to vector field visualization, is the young tradition of advanced tensor visualization methods in the considered application areas. Users need to get used to the advantages of modern visualization techniques, and therefore need tools to *explore* the data so they can develop an intuition and construct new hypotheses. Therefore, it is important to link methods domain experts are already used to with novel techniques. The main challenges in visualizing three-dimensional tensor fields, and the resulting goals of our work are:

- Tensor data are hard to interpret. Thus, we provide an intuitive approach to the analysis of tensor data.
- Tensor visualization methods do not have a long tradition in their respective application areas. Thus, we provide well-known perspectives onto these data and link them with novel visualization methods.
- A lack of a-priori feature definitions prevents the use of automatic segmentation algorithms. Thus, we allow users to *find the unknown* and let them steer the visualization process.
- The stress tensors we are dealing with are symmetric 3D tensors described by six independent variables. Thus, effectively capturing all of this information with a single visualization method is practically not feasible. We therefore employ a feature-dependent hybrid visualization.

---

• A. Kratz, B. Meyer and I. Hotz are with Zuse Institute Berlin.  
E-mail: [kratz@zib.de](mailto:kratz@zib.de), [bjoern.meyer@zib.de](mailto:bjoern.meyer@zib.de) and [hotz@zib.de](mailto:hotz@zib.de)

## Contribution

To meet these goals, we present a new access to tensor fields. The major contributions of this paper are:

- *Introduction of shape space theory as basic means for feature designation in attribute space.* Previous work mostly concentrated on the properties of a specific tensor type. We introduce an intuitive way of finding tensor invariants that reflect relevant features. Building upon the idea of shape space, the challenging task of translating questions into appropriate invariants boils down to a basis change of shape space. Using concepts from stress analysis and including failure models, we present invariants for stress tensor fields together with common and new visualization techniques (Figure 2). However, our approach is extendable to the analysis of various types of symmetric second-order tensors.
- *Introduction of multiple linked views to tensor visualization.* Previous work mostly concentrated on only two dimensions and/or one particular visualization technique. We pursue the idea of providing various perspectives onto the data and propose visual exploration in attribute and object space. The concept of shape space serves as link between the abstract tensor and its visualization in attribute space. In object space, features are mapped to displayable entities and are explored in a three-dimensional hybrid visualization.

## 2 RELATED WORK

Besides work from tensor field visualization [3], our work is based on publications from multiple view systems [4] as well as from the visualization of multivariate data [5]. This review is structured according to our main contributions focusing on second-order stress tensors and their visualization in attribute (diagram views) and object space (spatial views).

**Tensor Invariants:** Central to our work is the finding that tensor visualization methods can be designed and parametrized by a specific choice of invariants, which are scalar quantities that do not change under orthogonal coordinate transformation. Considering and analyzing important invariants is common in many physical applications [6]. For analysis of diffusion tensors, [6] has been transferred to visualization [7]. In the same context, Bahn [8] came up with the definition of *eigenvalue space*, where the eigenvalues are considered to be coordinates of a point in Euclidean space. In this work, we use the term *shape space* referring to application areas such as vision and geometric modeling. Coordinates within this space describe a set of tensor invariants and are called *shape descriptor*.

**Diagram Views:** Only few visualization papers are related to using diagram views for tensors. Mohr's circle [9] is a common tool in material mechanics, being used to compute coordinate transformations. In visualization, it has been applied to diffusion tensors to depict the tensor's diffusivity [10] as well as to stress tensors [11]. Being a

known technique for domain experts, Mohr diagrams can ease the access to novel visualization methods. Directional histograms have been used to visualize the distribution of fiber orientations in sprayed concrete [12] and for diffusion tensors in terms of rose diagrams and 3D scatterplots of the major eigenvector angles [13]. To the best of our knowledge, combined views for tensors have not been presented previously.

**Spatial Views:** A common classification of spatial visualization methods for second-order tensors is to distinguish between local, global and feature-based methods.

Local methods use geometries (glyphs) to depict single tensors at discrete points. Shape, size, color and transparency are used to encode tensor invariants. Dense glyph visualizations use less complex geometries together with placement algorithms [14], [15], [16]. When only selected locations are examined (probing), more complex geometries can be used. A variety of glyph types have been presented, focusing on stress tensors [2], higher-order tensors [17] and perceptual issues [18], [19]. Although, local methods have the potential to depict the whole tensor information, they generally fail in giving an overview of the complete 3D tensor field.

In contrast, global methods present an overview and emphasize regional coherence. They can be classified into methods based on scalar and vector visualization, as well as hybrid methods. Scalar visualization methods that are used to visualize tensors are ray-casting [20], [21], [22] and splatting [23], [24]. The main challenge is the design of an appropriate transfer function. Kindlmann et al. [20], [21] define an opacity transfer function based on the isotropic behavior of the tensor field. Color and shading are defined by tensor properties such as orientation and shape. Inspired by this work, Hlawitschka et al. [22] focus on directional information for transfer function design to emphasize fiber bundle boundaries. Recently, Dick et al. [1] presented a colormapping for stress tensors in order to distinguish between compressive and tensile forces.

Vector visualization methods are used to depict the behavior of the eigenvectors. We distinguish line tracing algorithms like tensorlines [25], texture-based approaches such as Line Integral Convolution (LIC) [26] and reaction-diffusion textures [27], [21]. Hotz et al. [28] presented a LIC-like method for the visualization of two-dimensional slices of a stress tensor field. They introduce a mapping of the indefinite stress tensor to a positive-definite metric. The mapped eigenvalues then are used to define input parameters used for LIC.

Whereas scalar-related visualization techniques are able to cover aspects of the whole 3D field, vector-related methods are mostly restricted to two dimensions. Hybrid approaches combine global and local methods [29], [30] as well as scalar- and vector-related techniques [1], [31]. Dick et al. [1] proposed hybrid visualization for 3D stress tensor fields. They combine ray-casting of the three eigenvalues with tensorlines to depict selected directions. To account for clutter, tensorlines are only seeded on a surface mesh. Although some hybrid approaches try to combine complex focus with non-disruptive context visualization, none of the existing methods allows the analysis and visualization of a complete 3D field both in detail and at

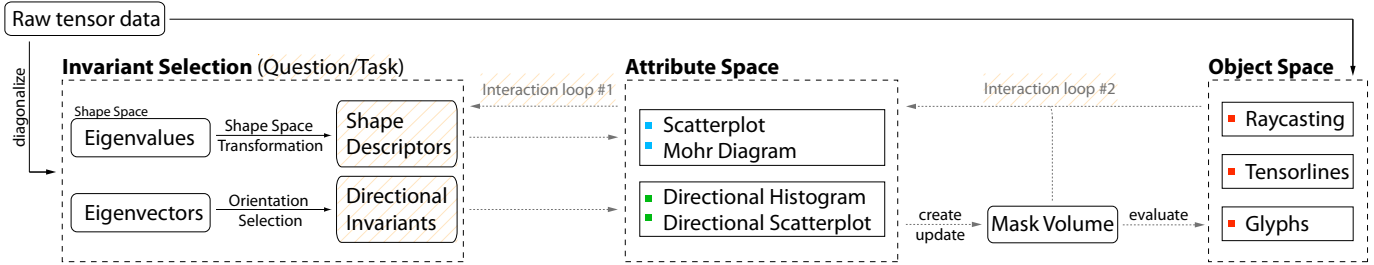


**Fig. 1:** Tensor analysis and visualization pipeline. The basis builds the diagonalization of the tensor into its eigenvalues and eigenvectors. The first step then is the choice of appropriate shape descriptors and directional invariants steered by a specific question or task. These are visualized in attribute space. Within this space, features are selected using brushing techniques and are then encoded in a mask volume. In object space, various tensor visualization techniques are combined in a feature-driven hybrid visualization. Volume rendering provides context, and glyphs or tensorlines are placed in focus regions. The user has a variety of options to adjust the visualization (interaction loops): Shape descriptors and directional invariants can be adapted (#1) and focus/context regions can be interactively refined (#2).

large.

Feature-based methods comprise topological methods [32], [33], [34], [35] and tensor segmentation algorithms [36], [37]. Regions of similar behavior are merged, which helps to handle the complex information within a tensor field. However, automatic segmentation algorithms can only be used, if the characteristics of interesting structures can be defined in advance. They fail in describing new features and might even remove important aspects of the data [5]. Furthermore, they are hard to extend to three-dimensional tensor data.

### 3 TENSOR VISUALIZATION AND ANALYSIS PIPELINE

Multiple linked views are used to explore three-dimensional stress tensor fields. We distinguish between diagram views in *attribute space* (see Section 5) and three-dimensional spatial views in *object space* (Section 6). Both are linked over a *mask volume*, i.e., a three-dimensional data structure of the same size as the input data storing a binary value (0 or 1). The mask is created and modified by brushing tensor properties in attribute space; it is evaluated for rendering in the spatial domain. For an overview of the proposed pipeline see Figure 1.

The basis of the pipeline is the diagonalization of the tensor (Section 4.1.1). Thus, the tensor is decomposed into *shape* and *orientation*, whereas shape refers to the eigenvalues and orientation to the eigenvectors. The first step then is the choice of appropriate shape descriptors and directional invariants (Section 4). We conceive this process as translating a question into a mathematical description (Figure 2). Being supported by various views in attribute space, the user can select and substitute tensor properties (interaction loop #1) until a set is found for being explored in more detail. Multiple views are possible at the same time, so different parameter choices and selections can be visually compared. Within these views, features are selected and highlighted using brushing-and-linking techniques (interaction loop #2). In this work, we propose the following diagrams: Shape space scatterplots can be understood as a cut through three-dimensional

shape space and, thus, deliver insight into the distribution of tensor properties (Section 5.1). Mohr diagrams [11] represent the most important invariants for stress tensors (Section 4.4). Directional histograms are used to analyze the distribution of principal directions (Section 5.3), and directional scatterplots to inspect shape properties together with directions (Section 5.4).

Hybrid object space rendering (Section 6) allows the inspection of the selected features in a spatial context. The mask defines in which regions glyphs are displayed and/or tensorlines are started. Volume rendering of scalar invariants serves as a context view. If the final image does not show all relevant features, users may refine their selections in attribute space, changing the mask volume and the rendering accordingly. Selections in object space, for example of single glyphs, are part of our future work.

## 4 TENSOR INVARIANTS AND SHAPE SPACE

In this section we formulate the task of finding relevant features in the language of shape space. Then we discuss our particular choice of shape descriptors, directions (Section 4.4) and shape space scaling (Section 4.3) for stress tensor fields.

### 4.1 Foundations

For the three-dimensional Euclidean space, a tensor  $T$  with respect to a basis  $(b_1, b_2, b_3)$ , denoted by  $T_b$ , can be described by a matrix  $M \in \mathbb{R}^{3 \times 3}$ . That is,  $T_b = M = (m_{ij})$  with  $i, j = 1, 2, 3$ . A tensor field over some domain  $D$  assigns a tensor  $T(x)$  to every point  $x \in D$ .

Tensor invariants are scalar quantities that do not change under orthogonal coordinate transformation. In general, any scalar function  $f(\lambda_1, \lambda_2, \lambda_3)$  again is an invariant. Most common examples are the tensor's eigenvalues, determinant and trace.

Question	Invariants		Scaling	Visualization Technique	Space	
	Shape	Orientation			Attribute	Object
Distinguish regions of compression, expansion, shear and isotropic regions.	$\sigma_1, \sigma_2, \sigma_3$		Logarithmic (SP)	Scatterplot	X	
Explore regions of high shear and kind of anisotropy.	$\tau, R$		Logarithmic (SP)	Scatterplot	X	
Distinguish regions of compression, expansion, shear. Kind of anisotropy. Tensor as a whole.	$\tau, C, R$		Linear (SP)	Mohr Diagram	X	
Distribution of principal directions.		$e_1, e_2, e_3$	-	Directional Histogram	X	
Distribution of directions of maximum shear stress.		$(e_1 \pm e_3)$	-	Directional Histogram	X	
Provide a spatial context by means of a derived scalar field.	$f(\sigma_1, \sigma_2, \sigma_3)$		Linear (SP)	Volume Rendering		X
Encode whole tensor information in focus regions.	$\sigma_1, \sigma_2, \sigma_3$	$e_1, e_2, e_3$	Asymmetric (POS)	Ellipsoid Glyph		X
Depict the normal stress acting at a given point in any direction.	$\sigma_1, \sigma_2, \sigma_3$	$e_1, e_2, e_3$	Linear (SP)	Reynolds Glyph		X
Depict the magnitude of shear stress acting at a given point in any direction.	$\tau$	$(e_1 \pm e_3)$	Linear (SP)	HWY Glyph		X
Emphasize selected directions.		$e_1, e_2, e_3$	-	Tensorlines		X
DTI example: Which regions exhibit high anisotropy, and do they have a characteristic shape?	$FA, mode(T)$	$e_1, e_2, e_3$	Normalized	Superquadric Glyph		X

**Fig. 2: Invariant Selection.** The table gives examples for shape descriptors and directional invariants that correspond to a specific task or question. We mainly present invariants for stress tensors. However, our approach is extendable to various types of symmetric second-order tensors. Besides convertible invariants, the analysis of tensors from diverse application areas requires variable scalings. The abbreviations SP and POS refer to sign-preserving mappings (SP) and mappings into a positive-definite metric (POS), respectively. Furthermore, the table lists possible visualization techniques in attribute and object space.

#### 4.1.1 Tensor Diagonalization

Tensors are *invariant* under coordinate transformation, which distinguishes them from matrices. That is, the characteristics of the tensor stay the same, independent from the choice of basis. Consequently, a tensor can be analyzed using any convenient coordinate system.

In the following, we only consider symmetric tensors, i.e.,  $m_{ij} = m_{ji}$ , being defined by six independent components. They can be transformed into a principal coordinate system using the concept of eigenanalysis

$$U T U^T = \begin{pmatrix} \lambda_1 & 0 & 0 \\ 0 & \lambda_2 & 0 \\ 0 & 0 & \lambda_3 \end{pmatrix}. \quad (1)$$

The diagonal elements  $\lambda_i$  are the eigenvalues and the transformation matrix  $U$  is composed of the eigenvectors  $e_i$ . For symmetric tensors, the eigenvalues are all real, and the eigenvectors constitute an orthonormal basis. They are ordered such that  $\lambda_1 \geq \lambda_2 \geq \lambda_3$ .

#### 4.1.2 Stress Tensor

A stress tensor conveys information about the stress acting on cutting planes through a material (Figure 3). It is given as

$$\sigma = \begin{pmatrix} \sigma_{11} & \tau_{12} & \tau_{13} \\ \tau_{12} & \sigma_{22} & \tau_{23} \\ \tau_{13} & \tau_{23} & \sigma_{33} \end{pmatrix}, \quad (2)$$

with the diagonal components  $\sigma_{ij}$  being the *normal stress* components and the off-diagonal components  $\tau_{ij}$  the *shear stress* components respective to cutting planes normal to the coordinate axis. The sign of the normal stress components

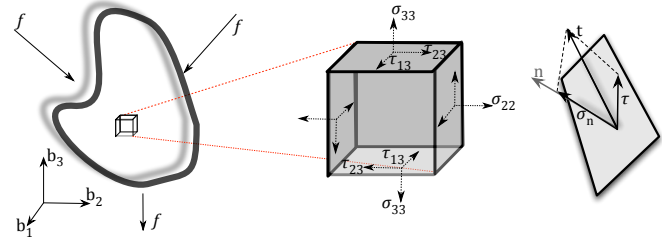


**Fig. 3: External forces  $f$  that are applied to a material (left), stress measured on an infinitesimally small volume element (middle), and force (traction  $t$ ) acting on an cutting plane with normal vector  $n$  (right).**

encodes if they are compressive or tensile. In this paper, we interpret negative eigenvalues as compressive forces (making the volume smaller) and positive eigenvalues as tensile forces (expanding the volume). It is worth noting that in some application areas the sign is interpreted in a reverse way. If forces are balanced and there is no rotation (which is, in general, fulfilled for infinitesimally small volume elements), the tensor is *symmetric* and uniquely described by its three eigenvalues and eigenvectors (Equation (1)). In this context, the eigenvectors are called principal stress axes, and the eigenvalues are called principal stresses. As principal stresses may be positive or negative, the tensor is indefinite. The force (traction vector)  $t$  acting on a cutting plane with normal vector  $n$  is given by

$$t = \sigma \cdot n = \tau + \sigma_n. \quad (3)$$

It can be decomposed into its normal stress  $\sigma_n$  and shear stress component  $\tau$  (Figure 3, right). In cutting planes orthogonal

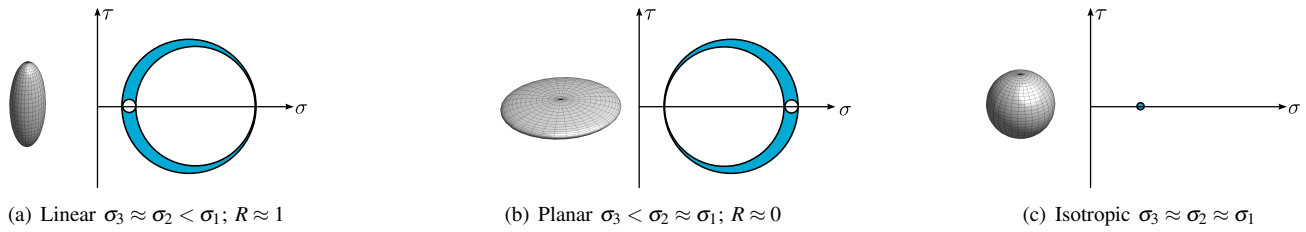


**Fig. 4:** Lamé's stress ellipsoid (displaying all possible traction vectors) and Mohr's circle in comparison. The ellipsoid's axes are aligned with the three eigenvectors, which are scaled by the eigenvalues. For three-dimensional tensors, Mohr's circle consists of three circles drawn between the three eigenvalues [11]. The horizontal axis depicts the normal stress and the vertical axis the shear stress. The outer circle gives an impression of the maximum shear stress, i.e., the larger the circle, the greater the shear stress acting on that plane. The blue shaded area represents all possible combinations of normal and shear forces for a given cutting plane. A point within this region then corresponds to the orientation of the plane's normal.

to the principal directions the shear stress vanishes. For planes with normals bisecting the minimum and maximum principal direction, the shear stress takes its maximum value and is called *maximum shear stress*  $\tau_{\max}$ . The corresponding directions are called *direction of maximum shear stress*.

## 4.2 Shape Space

We use the term shape space for the vector space spanned by the three eigenvalues. In this space, tensor shape [7] is represented by a point, whose coordinates are called shape descriptors. Finding shape descriptors, suiting the initial question, then corresponds to finding an appropriate reference frame (Figure 5). Common orthogonal reference frames correspond to Cartesian, spherical, and cylindrical coordinates, respectively. An example for a complete orthogonal spherical invariant set commonly used in the context of diffusion tensor imaging (DTI) is [7]: tensor norm (radius), fractional anisotropy (polar angle) and tensor mode (azimuthal angle). These descriptors represent central physiological properties (Figure 2). It is worth noting that all angular coordinates correspond to relative entities and are not defined in the origin ( $\text{norm}(T)^2 = \lambda_1^2 + \lambda_2^2 + \lambda_3^2 = 0$ ). For tensors with small norm, these values are unstable and sensitive to small changes. As a consequence, such coordinate systems are not optimal for indefinite tensors, for which the characteristic invariants may be positive, negative, or equal to zero (Section 4.1.2).

An additional useful property of a reference frame is orthogonality. Orthogonal invariants exhibit maximum independence of the shape descriptors by isolating changes of one invariant from variations of the others.

Which shape descriptors to use may depend on a variety of criteria. We propose the use of descriptors that give answers to specific questions and that are familiar to domain-experts. These criteria do not necessarily coincide with the mathematically most appealing choices.

## 4.3 Shape Space Scaling

The scale of the shape space's coordinate axes has a high impact on the visualization result. Therefore, it plays a crucial role in the diagram views (Section 5), as well as for rendering in the spatial domain (Section 6), where tensor invariants define color, transparency, glyph shape and glyph size. Most

common visualization methods require positive values, which is challenging for indefinite tensors, where the sign of the invariants reveals important physical characteristics. On the other hand, most diagram views are based on positive as well as negative eigenvalues. An optimal mapping depends on the given dataset and the desired visualization. It is possible to apply the mapping before choosing appropriate shape descriptors (holds for relative entities), or afterwards. We distinguish between the following mappings:

- Sign-preserving mappings (SP): Examples are linear and logarithmic mappings (Equation 6) as well as histogram equalizations.
- Mapping to  $\mathbb{R}^+$  (POS) [28], [38]: Values are mapped to the positive domain in a way that keeps the distinction between positive and negative values (Equation 7).

These mappings are further discussed in Sections 5 and 6 in the context of the specific visualization methods. The eigenvectors are already normalized and, therefore, do not need a mapping.

## 4.4 Shape Descriptors and Directions for Stress Tensors

Typical questions related to stress tensors are concerned with stability and failure analysis. Therefore, most failure models build on the analysis of the maximum shear stress. An example is the *Coulomb-Mohr failure criterion* [39]. Assuming no internal friction ( $\mu = 0$ ), it states that a material yields as long as the maximum shear stress  $\tau$  falls below the *intrinsic shear strength*  $\tau_0$  of the material. Figure 6 depicts this failure criterion graphically. As long as Mohr's circle (Section 5.2) does not intersect the failure line, the inspected material does not fracture. The normal of the corresponding fracture plane is the angle bisector of the principal directions of  $\sigma_1$  and  $\sigma_3$ : the direction of maximum shear stress. The material parameters  $\mu$  and  $\tau_0$  are measured in experiments.

Shape descriptors corresponding to the Coulomb criterion are [39]:

$$\begin{aligned}
 \tau &= \frac{\sigma_1 - \sigma_3}{2} \text{ maximum shear stress} \\
 c &= \frac{\sigma_1 + \sigma_3}{2} \\
 R &= \frac{\sigma_1 - \sigma_2}{\sigma_1 - \sigma_3} \text{ shape factor.}
 \end{aligned} \tag{4}$$

For other failure models, other shape descriptors exist. In general, these sets are not simple orthogonal coordinate frames, but represent important physical quantities.

Considering Mohr's circle,  $c$  represents its center, and  $\tau$  its radius (Figure 5). The shape factor  $R \in [0, 1]$  reveals the kind of anisotropy. Similar to the terminology used in DTI, stresses with  $R = 0$  are called *planar* and  $R = 1$  are called *linear* (Figure 4). It is a relative value and undefined for small values of  $\tau$  (isotropic stresses).

An example for another common anisotropy measure considering all principal stresses is the *von Mises stress*

$$\sigma_v = \sqrt{0.5 \cdot ((\sigma_1 - \sigma_2)^2 + (\sigma_2 - \sigma_3)^2 + (\sigma_1 - \sigma_3)^2)}. \quad (5)$$

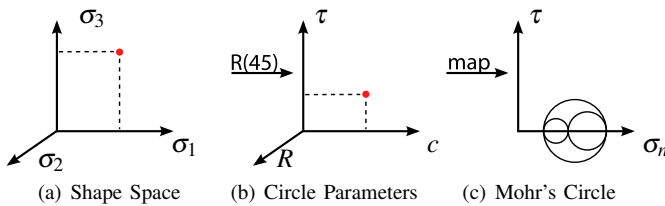


**Fig. 5:** Shape Space Transformation using the example of Mohr's Circle. The shape space (a) is spanned by the major (x-axis), minor (y-axis), and medium eigenvalue (z-axis). The tensor's shape is represented by a point. A circle is described by its center  $c$  and its radius, which corresponds to the maximum shear  $\tau$ . These shape descriptors are computed by a change of basis, which corresponds to a rotation around the  $\sigma_2$ -axis by 45 degrees (b). A final step corresponds to a mapping of  $(\tau, c, R)$  to glyph geometry (c), whereas  $R$  distinguishes planar and linear stresses.

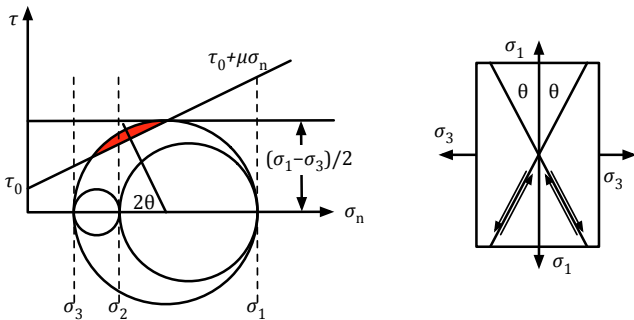


**Fig. 6:** Coulomb-Mohr failure criterion: The red area indicates normal-shear force combinations leading to material failure (left). The relation between the principal stress directions  $\sigma_1$  and  $\sigma_3$  and the predicted fracture plane are given by the angle  $\theta$ .

## 5 DIAGRAM VIEWS

We propose several diagram views, presenting various perspectives onto (stress) tensor characteristics (Figure 2). The views

abstract from the tensor volume's spatial representation, and give insight into the statistical distribution of tensor properties. All attribute-space views are linked and can be used side-by-side. Brushing in the views creates and updates a mask volume that is used to assign visualization methods in the spatial view (Section 6). The diagram views are parameterized by:

- Choice of shape descriptors.
- Choice of directions.
- Choice of shape space scaling.

In this section, we offer a default selection of views and parameterizations for the failure analysis of stress tensors. Of course, a wide range of other parameter choices corresponding to the underlying application and data is possible, too.

Statistical views (e.g. scatterplots, histograms) are especially suitable to quantify tensor characteristics. We have adapted scatterplots to fit scalar (Section 5.1) as well as directional tensor invariants (see Section 5.4). Directional histograms quantify selected directions, as eigenvectors or the direction of maximum shear. Furthermore, we present Mohr diagrams (Section 5.2) as additional perspective on the tensor data. They are a common tool in engineering, and therefore familiar to a large group of users. Compared to quantitative techniques, they give a more detailed view onto single tensors.

### 5.1 Shape Space Scatterplot

A scatterplot is used to depict the relation between two scalar invariants. Figure 7 illustrates a scatterplot that is used to quantify normal (compressive or tensile) and shear stresses. The input, therefore, are the three principal stresses sorted in descending order, i.e.,  $\sigma_1 \geq \sigma_2 \geq \sigma_3$ . The plot is divided into four quadrants (A,B,C,D). Due to the ordering, there never will be any points in the upper left quadrant (A). Points in the upper right quadrant (B) correspond to eigenvalues that are all positive, characterizing tensors of high tensile stresses. Accordingly, points in the lower left quadrant (C) correspond to high compressive stresses. The most interesting region is the lower right quadrant (D), which shows tensors with tensile and compressive stresses.

To summarize, we can deduce the following tensor field characteristics from the  $(\sigma_1, \sigma_3)$ -scatterplot:

- The more points in quadrant B, the higher the level of expansion.
- The more points in quadrant C, the higher the level of compression.
- The more points in quadrant D, the higher the level of mixed stresses.
- Points that have a large distance to the isotropic axis exhibit a high level of shear.
- Points that are located near the isotropic axis exhibit no shear at all; they describe tensors with isotropic behavior.

For the scatterplot, there is no need for a mapping into the positive domain. In contrast, an explicit distinction between positive and negative scalar invariants can be important. We propose two sign-preserving mappings: Logarithmic and histogram equalization [40]. As a standard logarithmic mapping

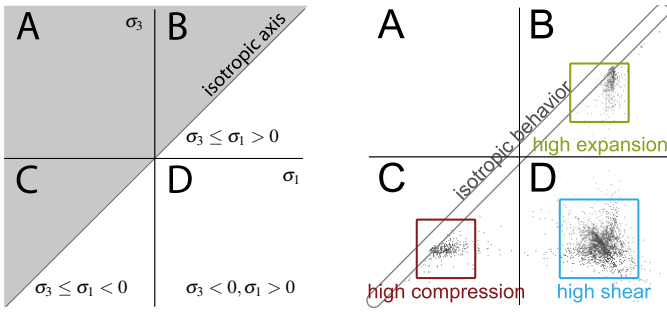


**Fig. 7:** Schematic illustration of the scatterplot (left). The  $x$ -axis represents the major eigenvalue and the  $y$ -axis the minor eigenvalue. The medium eigenvalue is color-coded (blue denotes low, red denotes high values). Example scatterplot for the two-force dataset (right); a simulation of a cube affected by a pushing and a pulling force, which results in compressive as well as tensile stresses. The eigenvalues were logarithmically mapped (Equation 6).

has a singularity in zero, we use

$$f(\sigma_i) = \begin{cases} \log(\sigma_i + 1), & \text{for } \sigma_i \geq 0 \\ -\log(1 - \sigma_i), & \text{for } \sigma_i < 0. \end{cases} \quad (6)$$

The results are then linearly mapped to the range of -1 to 1. In order to see as many tensor characteristics as possible, often a logarithmic mapping is sufficient. For some datasets, however, the data remain cluttered after the mapping. In this case, a histogram equalization is useful. Our modular approach allows an interactive adjustment of the mapping to the needs of the underlying dataset.

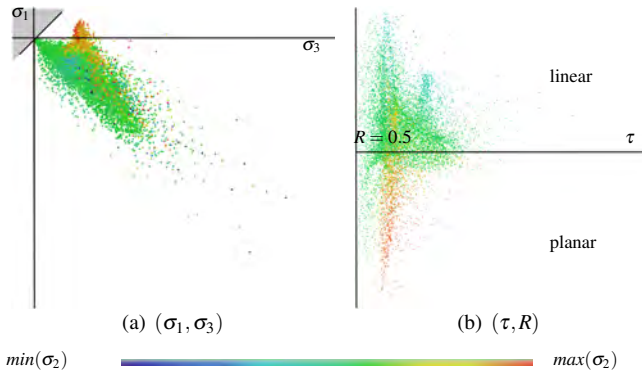


**Fig. 8:** Scatterplot for the slit-cube dataset (Section 7) with varying shape descriptors as input. (a) Considering  $(\sigma_1, \sigma_3)$  as input, regions of compression, expansion and shear can be distinguished. The inspected dataset exhibits mostly high shear stresses, no compressive forces and marginally tensile forces. Therefore, we analyze the shear region (Quadrant D) in more detail (b) considering  $(\tau, R)$ . Plotting the shape factor  $R$  reveals that within this region more linear ( $R \approx 1$ ) than planar ( $R \approx 0$ ) behavior happens.

## 5.2 Mohr Diagram

Figure 9 illustrates the Mohr diagram, which is used to analyze selected tensors in more detail. It consists of Mohr

circles (Figures 4 and 6), which give an impression of the relationship between the three eigenvalues and their relative strength. The circle's position on the  $x$ -axis indicates whether the respective tensor exhibits tensile or compressive forces. Its radius expresses the level of shear. In the original diagram [11], most circles would be located around the origin. This is a region of high interest as it represents high shear and sudden changes from tensile to compressive stresses. To equalize the circles' distribution, we exploit that, in general, a Mohr diagram is only one-dimensional; all circles are centered at the  $x$ -axis. We categorize the circles according to the tensor's anisotropic behavior (isotropic, linear, planar), and divide the Mohr diagram into three separate diagrams (Figure 9). Thus, clutter around the origin is reduced significantly. By drawing semi-circles in context regions, we achieve a more compact visualization without losing information or clarity. To summarize, we can deduce the following conditions from the Mohr Diagram:

- The more circles on the left, the higher the level of compression.
- The more circles on the right, the higher the level of expansion.
- Circles around the origin exhibit both: compressive and tensile forces.
- The greater the circle's radius, the higher the level of shear.
- Circles degenerating to a single point exhibit no shear at all; they describe tensors with isotropic behavior.
- A high number of circles on one of the three categorization axes represents a high number of isotropic/linear/planar tensors.

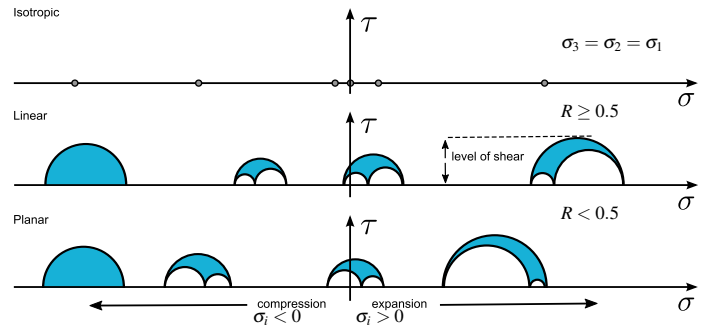


**Fig. 9:** We extended the Mohr diagram proposed by [11] as depicted above. The circle's position on the  $x$ -axis represents whether the corresponding tensor is in compression (left) or tension (right). The vertical position corresponds to their anisotropic behavior. For a better overview, we only draw semi-circles.

Due to its usability for the analysis and depiction of a single tensor or only a few tensors, the Mohr diagram is best used after a selection has been specified in the other diagram views. We achieve a further reduction of Mohr circles to be displayed, by clustering tensors with similar eigenvalue behavior. As similarity measure we use the Euclidean distance between two points in shape space. In the Mohr diagram, we encode the number of occurrences by color (Figure 13).

### 5.3 Directional Histogram

Figure 10 illustrates the directional histogram, which is used to analyze the distribution of principal shear directions. Of course, other directions of interest can be inspected, too. An example is the directions of maximum shear stress. The spherical diagram projects each direction, for example the major eigenvector, onto the surface of a unit sphere. Due to the non-oriented nature of a symmetric tensor's directional components only half of the sphere's surface needs to be considered. Therefore, all vectors are flipped to the positive half space of a user-selected axis  $(x, y, z)$ . To create the histogram, either a binning or a splatting approach [12] can be followed. We use the former. The number of intersections between vectors and a given surface patch on the sphere are counted, thus performing a region-dependent binning. For accurate results, a uniform subdivision of the surface is crucial. To account for patch size variations, we normalize the counted frequencies by the respective patch's surface area. Given a triangulation of the unit sphere, we either bin by triangle or by the Voronoi cell of each vertex. Triangle binning results in a discrete visualization of the counted frequencies, where each triangle is colored uniformly. Mapping the frequencies to vertex colors produces a continuous diagram, as the values are interpolated between neighboring vertices. The interpretation of the final plot depends on the selected viewing direction. In the 2D plot, the diagram's center corresponds to all vectors that are collinear with this viewing direction. An arbitrary point on the sphere's surface represents all vectors that span the angles  $\alpha$  and  $\beta$  with respect to the two axes orthogonal to the selected viewing direction (Figure 10).

We use two representations of the directional histogram (Figure 19):

- Hemisphere
- Mapping of the hemisphere into a planar representation for a better depiction in 2D [41]

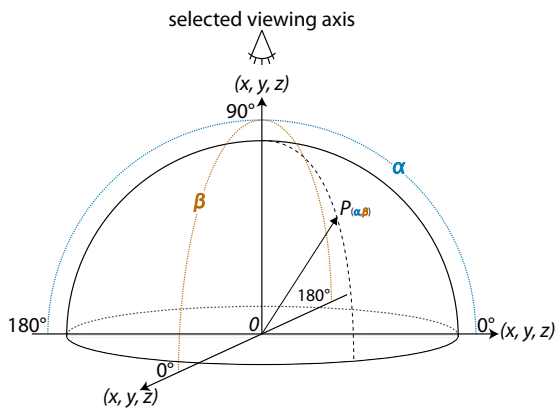


**Fig. 10:** The input directions for directional histogram and directional scatterplot are projected on a hemisphere, flipping all vectors to the half space defined by the selected viewing axis. Each point  $P_{(\alpha, \beta)}$  on the hemisphere represents all vectors spanning the angles  $\alpha$  and  $\beta$ .

### 5.4 Directional Scatterplot

The directional scatterplot uses the same setup of unit sphere and projected vectors as the directional histogram, but instead of binning the directions each vector is represented by an individual point on the sphere's surface. This direct representation of the vectors allows using the point's size, color, and transparency to represent tensor properties. Due to numeric instabilities in simulations, isotropic tensors exhibit an increased noise ratio (Figure 11, a). To reduce the noise level in the plot and emphasize pronounced directions, we map the shear stress to transparency. Thus, nearly isotropic tensors do not contribute to the final plot (Figure 11, b). Reasonable quantities to be mapped to colors are normal and shear stresses.

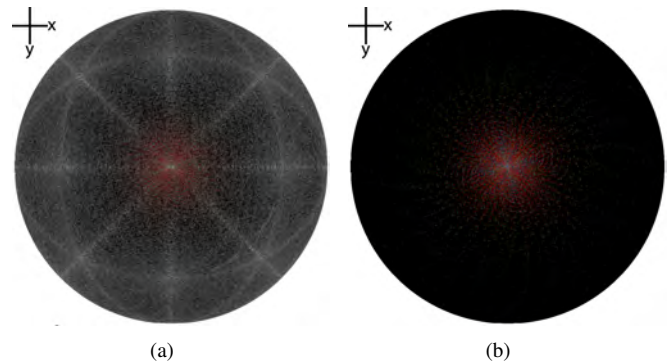


**Fig. 11:** Directional scatterplot for the rotating-star dataset. In Figure (a), all points have the same transparency, which reveals artifacts due to isotropic tensors. In Figure (b) the shear stress is mapped to transparency, i.e., low transparency for low shear stresses and nearly opaque points for high shear stresses. Thus, nearly isotropic tensors do not contribute to the plot.

## 6 SPATIAL VIEWS

The spatial views represent the tensor field in its original three-dimensional coordinates. The most basic method to display tensors in a spatial context is to use graphical icons (glyphs), e.g. ellipsoids, that are placed at discrete points within the volume. Although glyphs have the potential to show the entire tensor information, they fail to give a continuous view of the tensor field. Such a global view, however, is important to identify regions of compression and expansion, respectively. Volume rendering methods give a global view of the tensor field. However, in general they only work on derived scalar values and thus do not contain directional information. We use a hybrid rendering approach, combining volume rendering with glyphs and tensorlines. The visualization is interactively steered by a mask volume that is created and updated through user selections in the diagram views.

The basic idea is to use various visualization methods to separate focus and context regions in the dataset. Therefore, we evaluate the mask volume and map the selected features

to geometrical tensor representations (glyphs, tensorlines). The context is visualized by a volume rendering of the remaining dataset, using a scalar invariant chosen by the user.

**Volume Rendering:** Volume rendering serves as context view with decreased opacity in focus regions, allowing to analyze glyphs and tensorlines in more detail. We use standard GPU ray-casting of scalar invariants, for example, the von Mises stress. As tensorlines and glyphs are explicit geometries, we have to account for correct intersections between volume and opaque scene geometry. As proposed by [42], we use a depth image of the geometry. During volume traversal, rays are stopped as soon as they hit geometry positions.

**Tensorlines:** To add directional information, tensorlines can be drawn in focus regions, i.e., seeds are randomly placed inside the masked volume. Starting at these seed points, the line is integrated using a fourth-order Runge-Kutta scheme. The integration is stopped as soon as the line runs into an isotropic region.

**Tensor Glyphs:** Alternatively, glyphs can be drawn in focus regions, encoding the whole tensor information locally. Currently, we use ellipsoids. In order to distinguish between positive and negative eigenvalues, we map the tensor to a positive-definite metric using an antisymmetric-mapping [28]:

$$f(\sigma_i, c, \alpha) = \exp(\alpha \arctan(c \cdot \sigma_i)). \quad (7)$$

The parameter  $c$  determines the slope of the function in the origin,  $\alpha$  is a scaling parameter. The glyph's size can be adapted using a global scale parameter.

## 7 RESULTS

We describe two visual analysis sessions by means of two datasets with diverse characteristics (Sections 7.1, 7.2). Whereas the slit cube simulation is an example where domain experts have clear questions, the rotating-star dataset demonstrates a case with less specific questions. All analyses were performed on a standard desktop PC, equipped with an Intel Core 2 Duo CPU with 3.0 GHz and a NVIDIA GeForce 8800GT GPU.

### 7.1 Exploring the Slit-Cube Dataset

The slit-cube dataset is generated via a finite element simulation of the deformation of a clamped cube with two slits. Surface forces are applied to the top and the side of the cube, which is fixed at the bottom. Figure 12 (a) illustrates this process. The images are rendered based on a uniform resampling of the dataset. The resolution of the tensor field is  $256 \times 256 \times 256$ . In this context, the stress tensor expresses the cube's response to the applied forces. Questions are:

- How does the material respond to the applied forces?
- Which forces act in the material?

In general, the von Mises stress  $\sigma_v$ , a scalar value that is derived from the stress tensor (Equation (5)), is used to predict yielding of materials. Regions where  $\sigma_v$  is high, are prone to material failure.

Figure 12 (b) shows a spatial view of the dataset, using a hybrid rendering to visualize focus and context. A volume

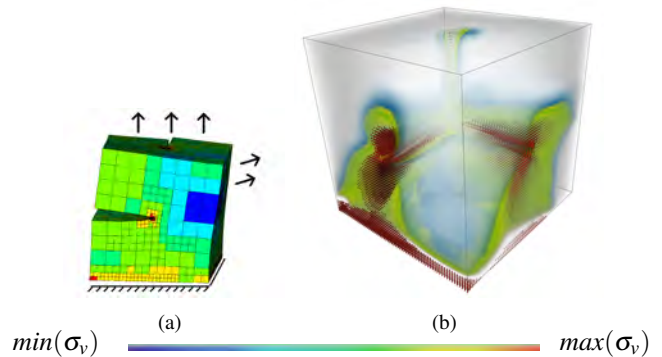


**Fig. 12: Slit Cube.** The dataset is based on a finite element simulation of the deformation of a clamped cube with two slits (a). It is fixed at the bottom. Surface forces act on the top and the side of the cube. (b) Shows a hybrid rendering of the slit-cube dataset. Volume rendering of the von Mises stress serves as context, while ellipsoids oriented by the eigenvectors and scaled by the eigenvalues are positioned in focus regions to emphasize high shear stresses.

rendering of the von Mises stress gives an impression of the whole field, while glyphs are positioned in focus regions and highlight areas of extremely high stresses. It can be seen that, due to the applied forces, the cube's slits increase. Large stresses are concentrated close to the edges of the slits and at the bottom where the cube is fixed, while large areas of the cube are hardly affected by the applied forces.

The von Mises stress is easy to interpret, however, important information of the stress tensor is ignored. That is, we cannot say which forces are prevalent in the material and we cannot say anything about the direction of maximum stresses.

The  $(\sigma_1, \sigma_2, \sigma_3)$ -scatterplot (Figure 8) allows a distinction between compressive, tensile and mixed stresses as well as isotropic and high shear stresses. It shows that the inspected dataset exhibits mostly indefinite stresses, no compressive forces and marginally tensile forces. Therefore, in the next step of the analysis, we switch the shape descriptors from  $(\sigma_1, \sigma_2, \sigma_3)$  to  $(\tau, R)$  using a logarithmical mapping (interaction loop #1) for the display (Figure 8). Thus, the shear region (Quadrant D) can be analyzed in more detail. Plotting the maximum shear stress against the shape factor  $R$  reveals that this region exhibits more linear than planar behavior. Linear, planar and isotropic stresses are further explored in the Mohr diagram (Figure 13). The circles are color-coded according to their frequency. Using the Mohr diagram as overview, we can reveal the physical behavior over the whole field. It is clearly visible that the slit-cube mainly exhibits indefinite stresses resulting in Mohr circles centered around the origin. However, looking at Figures 13 (b), (c) we can also deduce marginally compressive and tensile forces. As compressive forces are only small outliers in the scatterplot, we have not seen them before.

As we are especially interested in regions of high shear stress, we next examine the directions of maximum shear stress

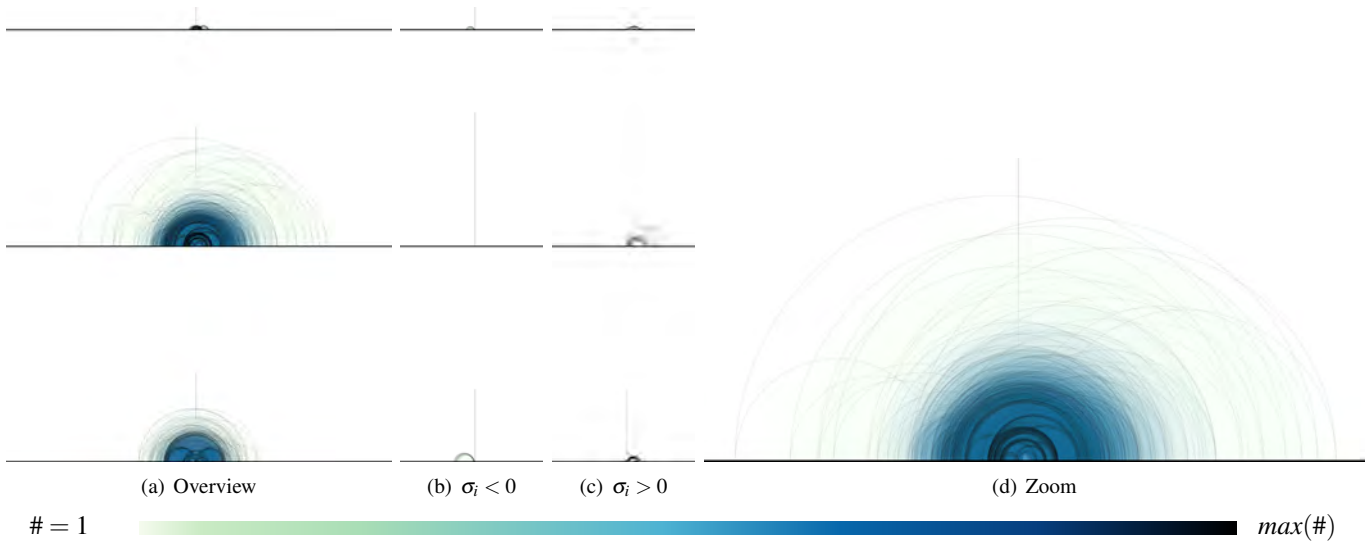
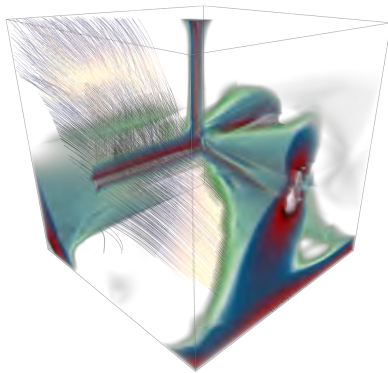


**Fig. 13:** *Slit Cube.* The Mohr diagram (a) mainly reveals mixed stresses (circles around the origin) as already shown in the scatterplot. Figures (b) and (c) show regions of compressive (b) and tensile forces (c), respectively. Looking at the scatterplot alone, we deduced that no compressive forces appear in the dataset, as these are only small outliers. Zooming into the linear region reveals more detail. The circles are colored according to their frequency (#).

(Figure 19). The directional histogram reveals one strongly expressed peak aligned with the  $z$ -direction. A second, minor accumulation is smeared over a larger angle in  $x,y$ -plane, approximately 90 degrees to the main stress direction. Figure 14 shows a hybrid rendering, where additional tensorlines are seeded in regions of high stress following the major principal stress direction.



$\min(\sigma_v)$    $\max(\sigma_v)$

**Fig. 14:** *Slit Cube.* The image shows a hybrid rendering of the slit-cube dataset. Volume rendering of the von Mises stress serves as context. Tensorlines are seeded in regions of high stress and integrated along the major eigenvector direction.

## 7.2 Exploring the Rotating-Star Dataset

Our second example shows data from an astrophysical simulation of a rotating neutron star's dynamics. Analyzing the evolution of such systems plays a major role for the understanding of the fundamental processes involved in core collapse supernovae and gravitational wave production.

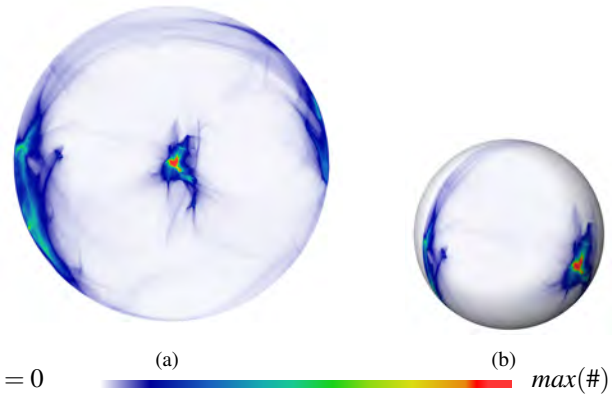


**Fig. 19:** *Slit Cube.* Directional histogram to examine the distribution of the directions of maximum shear stress. We mapped the hemisphere (front part of the sphere in (b)) into a planar representation (a) for a better depiction in the paper.

The simulation results consist of a variety of data types, i.e., (complex) scalars, vector fields and tensors. The data is usually three-dimensional and time-dependent, given on a grid with spatially varying resolution (AMR). In this work, we focus on the second-order stress tensor field. The data is resampled on a uniform grid with a resolution of  $128 \times 128 \times 128$  samples.

Until now, the domain experts' examination focused on the scalar fields (e.g. magnetic-, velocity- and density fields), which give insight into the evolution of the star formation. Other data types arise as intermediate product of the simulation. The additional analysis of the stress tensor field could support a deeper understanding of the physical processes that cause this specific formation. Investigations are, for example, related to the forces that participate in the star's

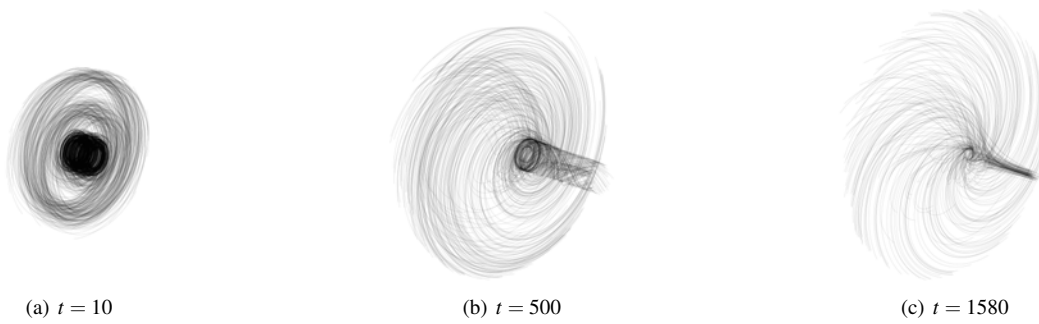


**Fig. 15:** Rotating Star. The tensorlines are integrated along the major eigenvector direction. Following the lines shows that the star's rotation lags around its perturbation. The seed points were placed at the star's center using a simple random seeding.

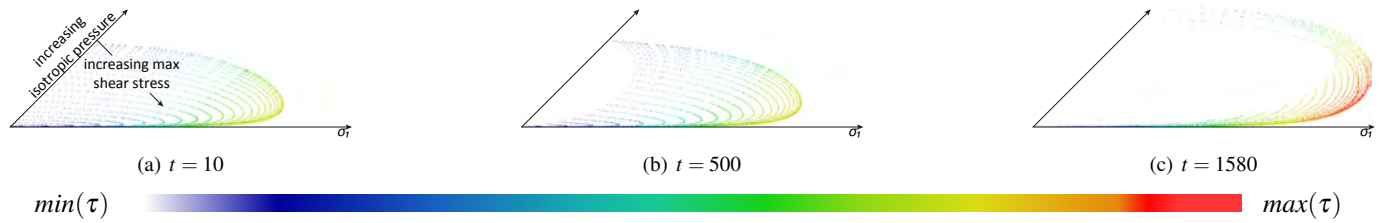


**Fig. 16:** Rotating Star. The scatterplot shows that, due to the perturbation, the forces get stronger with increasing time steps. The shape of the plot stays the same, which leads to the assumption that the eigenvalues correlate to each other. The color represents the maximum shear stress  $\tau$ .

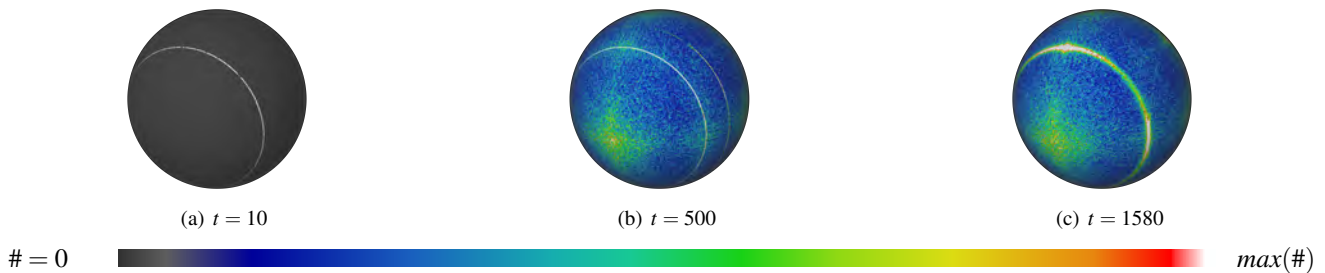


**Fig. 17:** Rotating Star. Directional histogram for the shear vectors. The colored triangles represent the number of data points ( $\#$ ) exhibiting a maximum shear direction falling into the triangle. At the beginning of the simulation (a) all shear directions exhibit a specific angle, which is nicely depicted by a single circle in the diagram. In later time steps, the shear directions become more scattered and the strongly expressed direction splits into two maxima rings (b). With further increasing time, these two maxima merge again resulting in one dominant ring (c). According to our domain experts, the splitting is not physical. It possibly reveals discretization artifacts.

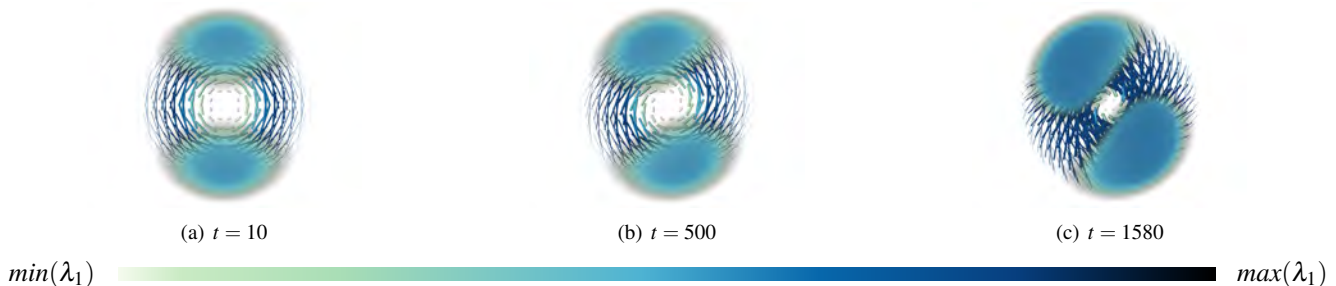


**Fig. 18:** Rotating Star. Hybrid rendering that combines volume rendering of the first tensor component with glyphs. Superquadrics are calculated only on the equatorial plane and colored according to the major eigenvalue  $\lambda_1$ . As deduced from the scatterplot, the forces get stronger with increasing time steps resulting in larger ellipsoids revealing linear forces.

collapse. However, contrary to our first example (Section 7.1), questions are much more basic. Since the users are not used to look at the tensor data, they do not have any specific

expectations. Therefore, the first goal of the visual exploration is to get an initial idea of the information that is contained in the data. Besides the physical interpretation, a thorough data

analysis is of high importance to validate the quality of the simulated data. Often, even simple visualizations can reveal failures in the simulations.

For a first impression of the dataset, Figure 15 displays tensorlines following the major eigenvector for three time steps  $t$ . The lines are seeded close to the center of the star.

Figure 20 shows the Mohr diagram of the rotating-star dataset. Due to the high gravitational forces inside the star only compressive stresses occur. According to our sign convention this means that all stresses are negative. In such a case it is common in the respective application areas to consider only the absolute value of the stresses. The principal stresses are ordered according to their magnitude, i.e.,  $|\sigma_1| \geq |\sigma_2| \geq |\sigma_3|$ . As a consequence, the dataset reveals positive-definite behavior, which can be clearly seen in the Mohr diagram. An interesting observation that can be made when zooming into the focus regions, is that the stresses exhibit perfectly linear behavior, i.e., the shape factor is  $R = 1$ .

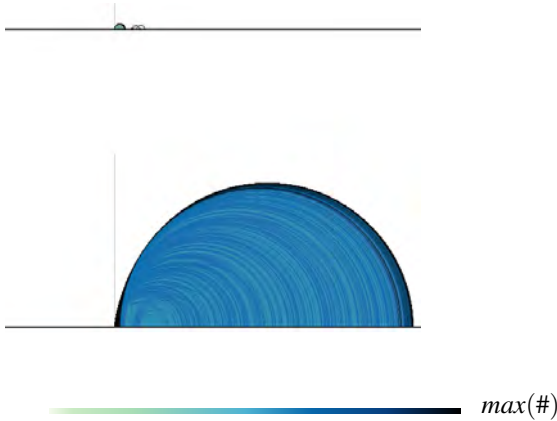


**Fig. 20:** Rotating star. The Mohr diagram reveals only compressive forces, which are perfectly linear. According to our sign convention this means that all stresses are negative. In such a case it is common in the respective application areas to consider only the absolute value of the stresses. The principal stresses are ordered according to their magnitude, i.e.,  $|\sigma_1| \geq |\sigma_2| \geq |\sigma_3|$  and, thus, restricted to the positive  $x$ -axis. In the selected region we draw full colored circles.

Figure 16 shows scatterplots for three time steps. As  $|\sigma_1| \geq |\sigma_2| \geq |\sigma_3|$ , only positive stresses occur. Therefore, only quadrant B is displayed. It can be observed that after the initial perturbation the principal stresses  $|\sigma_1|$ ,  $|\sigma_3|$  as well as the shear forces get stronger with increasing time, i.e., the distance to the isotropic axis increases (Figure 16 (c)). Interestingly the characteristic shape of the scatterplot stays the same over a long period of time. This might lead to the assumption that the major and minor eigenvalue correlate to each other. As we have seen in the Mohr diagram, all tensors exhibit perfect linear behavior. Therefore, we can deduce that the major eigenvalue  $|\sigma_1|$  grows almost quadratically with respect to  $|\sigma_2|$  and  $|\sigma_3|$ .

A temporal analysis of the dominant shear directions can be performed based on the directional histograms given in Figure 17. All time steps clearly reflect the symmetry inherent to the data set. At the beginning of the simulation ( $t = 10$ ) all shear directions exhibit a specific angle, which is nicely depicted by a single circle in the diagram. In later time steps, the shear directions become more scattered and the strongly expressed direction splits into two maxima rings ( $t = 500$ ). With further increasing time, these two maxima merge again resulting in one dominant ring ( $t = 1580$ ). According to our domain experts, the splitting is *not* physical. As a consequence, the visualization triggered a discussion about the possible reasons for this development. First ideas included discretization artifacts and problems with the resolution of the star's surface.

Figure 18 shows a hybrid rendering of the dataset. The volume rendering uses the  $\sigma_{11}$  component of the tensor. Even though this is not an invariant it expresses a characteristic tensor behavior, due to the high symmetry of the data. The rendering is combined with a glyph representation seeded in the equatorial plane.

## 8 DISCUSSION

Our results demonstrate the application of the presented pipeline (Figure 1) and shape space as basic means for feature designation in attribute space (Section 4). We have shown that the complexity of tensors can be embedded into a coherent concept, which builds the foundation for future research in tensor field visualization. Previous work mostly concentrated on one particular type of tensor and visualization technique. Analyzing tensors from diverse application areas, which exhibit different properties, requires convertible invariants and variable mapping techniques. Figure 2 shows invariants for stress tensors, however, the underlying concept can be used for other tensors, too. As motivated by our co-operation partners, future research will include the comparative visualization of different tensor types that occur during the same simulation (e.g. gravitational field tensor and stress tensor).

Our results and the discussion with domain experts further confirm the need for powerful visual exploration and analysis tools. The concurrent use of well known and new visualization methods provides an access to both, the data and modern visualization techniques. In material science and astrophysics, tensors are simulated solely to investigate scalar quantities (von Mises stress, density). Tensors mainly appear as intermediate product of simulations. Although, experts know that the tensor contains important information, which may help to answer their questions (What makes the material crack?, Which forces make the star collapse?), they avoid looking at the complex data as they do not know how to interpret it.

Until now, domain experts are mainly used to two-dimensional plots. Therefore, attribute-space plots are of

high importance. Our experience is that domain experts favor simple visualization techniques like scatterplots and icons that are familiar to them (e.g. Mohr's circle). In object space, a sparse usage of lines and glyphs at specific locations is preferred, which motivates the use of a binary mask volume to determine focus and context regions. Moreover, all physicists and engineers rated the brushing-and-linking as extremely helpful to ease the interpretation of the data. That way, the visual exploration leads to new questions, which encourages both, the curiosity to look at the whole tensor and, as a consequence, the development and usage of more complex visualization techniques. Another aspect that arose during discussions was the usefulness of our methods to detect failures in simulations.

Our material science partners really like the Mohr diagram; the familiar technique motivated them to use our tools. For astrophysicists the representation was new but considered as interesting. A limitation is that the diagram suffers from clutter. A clear distinction between linear and planar anisotropy in the tensor field is still difficult. Therefore, we will integrate clustering algorithms in the future to reveal more insight into important tensor properties.

Another subject that remains to be investigated is volume rendering in the context of tensor fields. Users like this visualization technique as they know, how to interpret it. This work presents renderings of scalar measures (e.g., von Mises stress). Recently, Dick et al. [1] presented a colormapping of the three eigenvalues to distinguish between compressive and tensile forces. More advanced colormappings based on other tensor invariants may be interesting, too.

## 9 CONCLUSION

To the best of our knowledge, we presented the first approach that solves the challenging problem of visualizing three-dimensional tensor fields by combining multiple views. A solid theoretical basis was provided by extending the notion of shape space, which serves as a link between the abstract tensor and its visualization in attribute space. This theory provides an intuitive way of finding relevant features.

In the considered application areas, visual tensor analysis and exploration are still in their infancy. Domain experts are often used to the analysis of derived scalar fields, although they know that the tensor field contains important information to their questions. Especially attribute plots help them to familiarize themselves with more advanced visualization techniques, explore the data and to construct new hypotheses.

## ACKNOWLEDGMENTS

This work was funded by the German Research Foundation (DFG) through a Junior Research Group Leader award (Emmy Noether Program). Rotating-star data supplied courtesy of Luca Baiotti from the Albert Einstein Institute (AEI). The slit-cube dataset was provided by Andreas Schroeder, Humboldt University Berlin. The authors would further like to thank

Markus Hadwiger, Aaryn Tonita, Michael Koppitz, Steffen Prohaska and our students David Bressler and Nino Kettlitz. Finally, we thank the reviewers for their valuable comments.

## REFERENCES

- [1] C. Dick, J. Georgii, R. Burgkart, and R. Westermann, "Stress tensor field visualization for implant planning in orthopedics," *IEEE Transactions on Visualization and Computer Graphics*, vol. 15, no. 6, pp. 1399–1406, 2009.
- [2] Y. M. A. Hashash, J. I.-C. Yao, and D. C. Wotring, "Glyph and hyperstreamline representation of stress and strain tensors and material constitutive response," *International Journal for Numerical and Analytical Methods in Geomechanics*, vol. 27, no. 7, pp. 603–626, 2003.
- [3] H. Hagen and C. Garth, "An introduction to tensors," in *Visualization and Processing of Tensor Fields*. Springer, 2006.
- [4] H. Doleisch, M. Gasser, and H. Hauser, "Interactive feature specification for focus+context visualization of complex simulation data," in *VISSYM '03: Proceedings of the symposium on Data visualisation 2003*. Eurographics Association, 2003, pp. 239–248.
- [5] R. Bürger and H. Hauser, "Visualization of multi-variate scientific data," in *EuroGraphics 2007 State of the Art Reports (STARs)*, 2007, pp. 117–134. [Online]. Available: <http://www.cg.tuwien.ac.at/research/publications/2007/buerger-2007-star/>
- [6] J. C. Criscione, J. D. Humphrey, A. S. Douglas, and W. C. Hunter, "An invariant basis for natural strain which yields orthogonal stress response terms in isotropic hyperelasticity," *Journal of the Mechanics and Physics of Solids*, vol. 48, pp. 2445–2465, 2000.
- [7] D. B. Ennis and G. Kindlmann, "Orthogonal tensor invariants and the analysis of diffusion tensor magnetic resonance images," *Magnetic Resonance in Medicine*, vol. 55, no. 1, pp. 136–146, 2006.
- [8] M. M. Bahn, "Invariant and orthonormal scalar measures derived from magnetic resonance diffusion tensor imaging," *Journal of Magnetic Resonance*, vol. 141, no. 1, pp. 68–77, 1999.
- [9] R. Brannon, "Mohr's circle and more circles," [http://www.mech.utah.edu/~brannon/public/Mohrs\\_Circle.pdf](http://www.mech.utah.edu/~brannon/public/Mohrs_Circle.pdf), 2003. [Online]. Available: [http://www.mech.utah.edu/~brannon/public/Mohrs\\_Circle.pdf](http://www.mech.utah.edu/~brannon/public/Mohrs_Circle.pdf)
- [10] M. Bilgen, I. Elshafiey, and P. A. Narayana, "Mohr diagram representation of anisotropic diffusion tensor in MRI," *Magn Reson Med*, vol. 47, pp. 823–827, Apr 2002.
- [11] P. Crossno, D. H. Rogers, R. M. Brannon, D. Coblenz, and J. T. Fredrich, "Visualization of geologic stress perturbations using mohr diagrams," *IEEE Transactions on Visualization and Computer Graphics*, vol. 11, no. 5, pp. 508–518, 2005.
- [12] L. Fritz, M. Hadwiger, G. Geier, G. Pittino, and M. E. Gröller, "A visual approach to efficient analysis and quantification of ductile iron and reinforced sprayed concrete," *IEEE Transactions on Visualization and Computer Graphics*, vol. 15, no. 6, pp. 1343–1350, Oct. 2009.
- [13] Y.-C. Wu, A. S. Field, M. K. Chung, B. Badie, and A. L. Alex, "Quantitative analysis of diffusion tensor orientation: Theoretical framework," in *Magnetic Resonance in Medicine*, 2004, pp. 1146–1155.
- [14] G. Kindlmann and C.-F. Westin, "Diffusion tensor visualization with glyph packing," *IEEE Transactions on Visualization and Computer Graphics*, vol. 12, no. 5, pp. 1329–1336, 2006.
- [15] M. Hlawitschka, G. Scheuermann, and B. Hamann, "Interactive glyph placement for tensor fields," in *ISVC (1)*, 2007, pp. 331–340.
- [16] L. Feng, I. Hotz, B. Hamann, and K. Joy, "Anisotropic noise samples," *IEEE Transactions on Visualization and Computer Graphics*, vol. 14, no. 2, pp. 342–354, 2008.
- [17] R. D. Kriz, E. H. Glaessgen, and J. MacRae, "Eigenvalue-eigenvector glyphs: Visualizing zeroth, second, fourth and higher order tensors in a continuum," *NCSA Workshop on Modeling the Development of Residual Stresses During Thermoset Composite Curing*, 1995.
- [18] G. Kindlmann, "Superquadric tensor glyphs," in *Proceedings of IEEE TVCG/EG Symposium on Visualization '04*, 2004, pp. 147–154.
- [19] C.-F. Westin, S. E. Maier, H. Mamata, A. Nabavi, F. A. Jolesz, and R. Kikinis, "Processing and visualization of diffusion tensor MRI," *Medical Image Analysis*, vol. 6, no. 2, pp. 93–108, 2002.
- [20] G. Kindlmann and D. Weinstein, "Hue-balls and lit-tensors for direct volume rendering of diffusion tensor fields," in *VIS '99: Proceedings of the conference on Visualization '99*. IEEE Computer Society, 1999.
- [21] G. Kindlmann, D. Weinstein, and D. Hart, "Strategies for direct volume rendering of diffusion tensor fields," *IEEE Transactions on Visualization and Computer Graphics*, vol. 6, no. 2, pp. 124–138, 2000.

- [22] M. Hlawitschka, G. Scheuermann, G. H. Weber, O. T. Carmichael, B. Hamann, and A. Anwander, "Interactive volume rendering of diffusion tensor data," in *Visualization and Processing of Tensor Fields: Advances and Perspectives*, ser. Mathematics and Visualization, D. H. Laidlaw and J. Weickert, Eds. Springer, 2009.
- [23] W. Bengler, H. Bartsch, H.-C. Hege, and H. Kitzler, "Visualizing neuronal structure in the human brain via diffusion tensor MRI," *Intern. Journal of Neuroscience*, vol. 116, pp. 461–514, 2006.
- [24] A. Bhalerao and C.-F. Westin, "Tensor splats: Visualising tensor fields by texture mapped volume rendering," in *MICCAI (2)*, 2003, pp. 294–302.
- [25] D. Weinstein, G. Kindlmann, and E. Lundberg, "Tensorlines: Advection-diffusion based propagation through diffusion tensor fields," in *Proceedings of IEEE Visualization 1999*, 1999, pp. 249–253.
- [26] X. Zheng and A. Pang, "Hyperlic," in *VIS '03: Proceedings of the conference on Visualization '03*. IEEE Computer Society Press, 2003, pp. 249–256.
- [27] A. R. Sanderson, M. Kirby, C. R. Johnson, and L. Yang, "Advanced reaction-diffusion models for texture synthesis," *Journal of Graphics Tools*, vol. 11, no. 3, pp. 47–71, 2006.
- [28] I. Hotz, L. Feng, H. Hagen, B. Hamann, K. Joy, and B. Jeremic, "Physically based methods for tensor field visualization," in *VIS '04: Proceedings of the conference on Visualization '04*. IEEE Computer Society, 2004, pp. 123–130.
- [29] D. H. Laidlaw, E. T. Ahrens, D. Kremers, M. J. Avalos, R. E. Jacobs, and C. Readhead, "Visualizing diffusion tensor images of the mouse spinal cord," in *VIS '98: Proceedings of the conference on Visualization '98*. IEEE Computer Society Press, 1998, pp. 127–134. [Online]. Available: <http://visinfo.zib.de/EVlib/Show?EVL-1998-331>
- [30] A. Sigfridsson, T. Ebbens, E. Heiberg, and L. Wigström, "Tensor field visualisation using adaptive filtering of noise fields combined with glyph rendering," in *VIS '02: Proceedings of the conference on Visualization '02*. IEEE Computer Society, 2002, pp. 371–378.
- [31] B. Zehner, "Interactive exploration of tensor fields in geosciences using volume rendering," *Computers and Geosciences*, pp. 73–84, 2006.
- [32] L. Hesselink, Y. Levy, and Y. Lavin, "The topology of symmetric, second-order 3D tensor fields," *IEEE Transactions on Visualization and Computer Graphics*, vol. 3, no. 1, pp. 1–11, Jan./Mar. 1997, diss. [Online]. Available: <http://www.computer.org/tvcg/tg1997/v0001abs.htm>;<http://dlib.computer.org/tg/books/tg1997/pdf/v0001.pdf>
- [33] X. Zheng and A. Pang, "Topological lines in 3d tensor fields," in *VIS '04: Proceedings of the conference on Visualization '04*. IEEE Computer Society Press, 2004.
- [34] X. Zheng, X. Tricoche, and A. Pang, "Degenerate 3d tensors," University of California, Santa Cruz, Tech. Rep. UCSC-CRL-04-09, 2004.
- [35] X. Tricoche, G. L. Kindlmann, and C.-F. Westin, "Invariant crease lines for topological and structural analysis of tensor fields," *IEEE Transactions on Visualization and Computer Graphics*, vol. 14, no. 6, pp. 1627–1634, 2008.
- [36] J. Sreevalsan-Nair, C. Auer, B. Hamann, and I. Hotz, "Eigenvector-based interpolation and segmentation of 2d tensor fields," in *Proceedings of Topological Methods in Visualization (TopoInVis'09)*, to appear 2010.
- [37] R. de Luis-Garca, C. Alberola-Lpez, and C.-F. Westin, "Segmentation of tensor fields: Recent advances and perspectives," in *Tensors in Image Processing and Computer Vision*, S. Aja-Fernández, R. de Luis García, D. Tao, and X. Li, Eds. Springer London, 2009.
- [38] R. M. Kirby, H. Marmanis, and D. H. Laidlaw, "Visualizing multivalued data from 2D incompressible flows using concepts from painting," in *Proc. Visualization*, 1999, pp. 333–340.
- [39] B. Lund, "Crustal stress studies using microearthquakes and boreholes," Ph.D. dissertation, Department of Earth Sciences, Uppsala University, 2000.
- [40] J. Blaas, C. Botha, and F. Post, "Extensions of parallel coordinates for interactive exploration of large multi-timepoint data sets," *IEEE Transactions on Visualization and Computer Graphics*, vol. 14, no. 6, pp. 1436–1451, Nov.-Dec. 2008.
- [41] D. Stalling and H.-C. Hege, "Fast and intuitive generation of geometric shape transitions," *The Visual Computer*, vol. 16, pp. 241–253, 2000.
- [42] K. Engel, M. Hadwiger, J. M. Kniss, C. R. Salama, and D. Weiskopf, *Real-Time Volume Graphics*. AK Peters, Ltd., 2006.